Instruments and Methods

Microstructural change around a needle probe to measure thermal conductivity of snow

Fabienne RICHE, Martin SCHNEEBELI

WSL Institute for Snow and Avalanche Research SLF, Flüelastrasse 11, CH-7260 Davos Dorf, Switzerland
E-mail: schneebeli@slf.ch

ABSTRACT. The thermal conductivity of snow determines, to a large extent, ground heat flux and snow metamorphism. One common method of measuring the thermal conductivity of snow is with a needle probe. We measured the microstructural changes in the snow around a typical needle using micro-computed tomography. The insertion of the needle probe caused structural changes up to a radial distance of 0.5–1 mm. Using a commercial needle probe with short (30 s) heating time, we measured thermal conductivity values in snow that were 50% lower than the conductivity measured using a calibrated guarded hot-plate apparatus. Numerically simulated time–temperature curves with an introduced air gap that simulated the needle damage reproduced the observed needle-probe results well, confirming that poor contact resistance between the needle and the snow will lead to measurement discrepancies and a large bias. While most measurements in snow have been done using a long heating time and are not subject to this error, the thermal conductivity of snow measured with needle probes with short measurement times should be avoided. This same effect is probably observed in other brittle and highly porous materials, a condition that may not be widely appreciated.

1. INTRODUCTION

Thermal conductivity is one of the most fundamental physical properties of snow and firn. It determines ground heat flux (Zhang, 2005; Cook and others, 2008) and radiation balance (Sturm and others, 2002), as well as electromagnetic properties (Koenig and others, 2007). Within the snowpack, thermal conductivity essentially determines the rate of metamorphism, because the rate of snow metamorphism is largely proportional to the temperature gradient. It is widely understood that the thermal conductivity depends on snow microstructure and density (Arons and Colbeck, 1995; Kaempfer and others, 2005). Common techniques used to measure thermal conductivity in snow are guarded heating plates (Pitman and Zuckerman, 1967; Schneebeli and Sokratov, 2004), needle probes (Lange, 1985; Sturm and others, 2002; Courville and others, 2007) and Fourier analysis of the propagating thermal waves (Brandt and Warren, 1997). Sturm and others (1997) reviewed the many published measurements of thermal conductivity of snow, and measured 488 samples over a wide density and structural range using needle probes (Sturm and Johnson, 1991). Sturm and others (2002) updated this dataset and it is considered the reference data for the thermal conductivity of snow.

Despite the extensive literature, measuring thermal conductivity of snow is challenging. All current models simulating the thermal behavior of snowpacks (Brun and others, 2008, p. 150; Cook and others, 2008) use parameterizations where the thermal conductivity is about twice as high for the same density as needle-probe measurements, a result noted by Sturm and others (2002), who at that time thought the discrepancy derived from three-dimensional (3-D) aspects of the heat transfer in snow; however, the cause is now under investigation by us and by Sturm and others. One possibility is an unusual interaction between the needle and anisotropy in the snow.

De Vries (1952) and Von Herzen and Maxwell (1959) introduced the needle-probe method of measuring thermal conductivity in soils and sediments. The method uses a single thin steel needle inserted in the material of interest. The needle is heated and the change in temperature during a heating and a cooling cycle is measured. Effectively, the probe mimics a transient-line heat source. Carslaw and Jaeger (1959) derived an analytical solution for this situation. Actually, two solutions can be used: The first is the Carslaw and Jaeger equation, a solution that was analyzed in detail for needle probes by Bristow and others (1994). It can be used for short ($\leq$30 s) heating time, but the value of the contact resistance between the needle and the medium must be known. The second solution is to make a longer measurement and then use the long-term equation of Blackwell (1956).

Here our focus is on examining the impact of inserting a needle probe into snow. We hypothesize that this action damages the snow and potentially produces an air-gap annulus. The impact of the air gap will depend on the length of the test, with short-time-solution needle measurements adversely impacted while longer tests will still be accurate. Nusier and Abu-Hamdeh (2003) indicate that the poor contact between the soil and the needle probe decreases the heat conductance around the needle probe, leading to an underestimate (Abu-Hamdeh, 2001). The detailed analysis by Ewen and Thomas (1987) shows that the error is related nonlinearly to the ratio of the heat capacity of the probe to that of the material (Fourier coefficient) and to the effect of contact resistance. While, to date, most needle-probe measurements in snow (e.g. Sturm and others, 2002; Courville and others, 2007) have used the long time solution, commercial needles are starting to be used for snow, and the air-gap problem remains for soils and other porous media.

Table 1. Physical and geometrical properties of the snow samples used. ISC: snow class (international snow classification 1990); #: number of snow samples; $1 - n$: ice fraction in snow; SSA: specific surface area; i.th: mean ice thickness; i.sp: mean ice pore space

Snow type	ISC	#	$1 - n$	SSA	i.th	i.sp
			%	mm^{-1}	mm	mm
New snow	1	1	9	45.6	0.08	0.40
Small rounded	3a	9	14	29.5	0.12	0.36
Cup crystals	5a	4	22	16.1	0.18	0.61
Large rounded	3b	4	27	11.6	0.27	0.58
Faceted	4a	4	27	9.3	0.35	0.75
Melt refrozen	6a	1	34	7.5	0.42	0.76

Until now the structural change caused by inserting a needle in a porous material could only be estimated by indirect methods, but now micro-computed tomography (μCT) allows 3-D visualizations at high resolution and characterization of materials in a non-invasive and non-destructive way (Ketcham and Carlson, 2001). We used a cooled μCT to observe snow and its structural changes before and after the insertion of a needle probe, following procedures described by Schneebeli and Sokratov (2004), without any foregoing casting. Our objective was to link the snow–needle contact at the microstructural level directly with the thermal behavior of the needle. A continuum finite-element model was used to simulate the observed temperature response. We show that the microstructure of snow around the needle is changed, and does not form an ideal contact. Therefore a needle with a short heating time should not be used in snow.

2. METHODS

2.1. Sample preparation

Twenty-one different natural snow samples, taken from different snow profiles, were used for the measurements. Two needle-shaped graphite rods of 1.2 mm diameter (Caran d'Ache Type 6177a, HB) were inserted in each sample, producing 42 μCT measurements in total. The samples included new snow, small rounded grains, faceted grains, large rounded grains, melt-refrozen snow and depth hoar. The samples varied in density, snow type and microstructure (Table 1). The graphite was used because a steel needle will create large artifacts in the reconstructed tomographic images due to total adsorption. The diameter of the 'needles' was the same as that used by Lange (1985), Sturm and Johnson (1991), Sturm and others (1997) and Courville and others (2007).

2.2. Micro-computed tomography and image processing

The snow was cut out carefully from larger samples without disturbance and vertically inserted into a sample holder 80 mm high and 36.9 mm in diameter. A temperature-controlled cooled μCT (Scanco micro-CT80) was used. The temperature in the μCT was kept constant at −15°C. The images had a nominal resolution of 18 μm. The scanned height was 7.5 mm (416 slices, each slice 2048 × 2048 pixels). First, the undisturbed snow was scanned in the sample holder. Then the two pointed carbon needles were inserted without wobbling, which was prevented by

mounting a 30 mm long guide on top of the sample holder. The guide had two 1.2 mm diameter boreholes, 14 mm apart. The same snow sample was then scanned a second time. The sample holder was not moved during insertion of the needle. A few experiments were also made with a horizontal insertion of the needle in snow, to see if the direction of the insertion affected the variation of the local volume fraction.

During the needle test the maximum temperature increase around the needle was 2 K, so no melting occurred. The pressure on the snow due to the insertion of the needle also did not cause any melting of the snow crystals.

To analyze the measurements, we used a volume of $600 \times 600 \times 400$ voxels (10.8 mm × 10.8 mm × 7.2 mm) around each needle insertion area. The reconstructed grayscale volume was used to observe single slices and the contact between the needle and the snow sample directly without image processing. This volume was segmented, and variations in ice volume fraction around the needle were calculated. The segmentation was done for the ice structure and the carbon needle separately, to minimize the effect of voxels containing both ice and needle. A Gauss filter and a threshold which was different for the ice volume and the needle volume was used. Because the snow structure is different from one snow type to another, these two parameters were chosen manually for each sample, minimizing the difference between grayscale image and segmented image. For the needle volume, the Gauss filter and threshold were kept constant (Gauss filter: $\sigma = 1$, support = 1; range 600–1000‰). An additional morphological opening was then applied to the needle volume to remove artifacts caused by voxels containing ice and needle.

The microstructural characterization we used for the snow samples is described by Kaempfer and Schneebeli (2007). Ice volume fraction of the sample, $1 - n$ (where n is pore fraction), the mean thickness of the snow structure, i.th, the mean thickness of the pores, i.sp, and the specific surface area, SSA, were all calculated.

The ice volume fraction, V_i, around the carbon needle was evaluated as a function of radial distance by creating an empty cylinder with an inner radius corresponding to the needle radius and 2 voxels (36 μm) wall thickness (Fig. 1). The radius of this cylinder was then increased by 2 voxels but keeping the same wall thickness. The cylinder was applied recursively until a maximum radius of 200 voxels (3.6 mm) was reached. To evaluate the local volume percentage at a known distance around the needle, the ice volume, V_I, was divided by the voxels of the cylinder, V_C, corresponding to the radial distance, and the result multiplied by 100 ($V_i = (V_I / V_C) \times 100$).
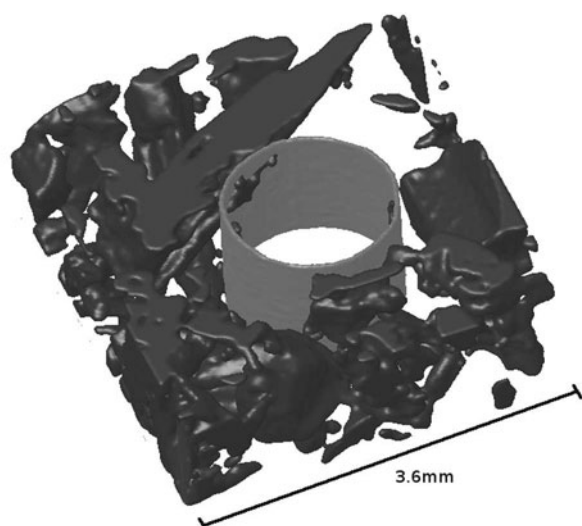
Fig. 1. Illustration of the density and density-change sampling procedure in the virtual snow. The image shows the snow structure (in dark gray) after inserting the needle, and the sampling cylinder (in gray, 180 μm from the edge of the needle). The needle is digitally removed. For illustrative purposes, only $3.6 \times 3.6 \times 0.72 \, mm^3$ of the total sampled volume of $10.8 \times 10.8 \times 7.2 \, mm^3$ is shown.

Because the volume fraction fluctuated around the bulk density of the snow sample computed for the full volume ($600 \times 600 \times 400$ voxels), the values were normalized: the volume fraction of the snow was evaluated from the first μCT measurement before the needle was inserted and from the second measurement after the needle was inserted. The ratio of these two volume fractions was then used to evaluate the change.

2.3. Measurement of thermal conductivity

To measure the thermal conductivity of the reference material and the snow samples, we used a KD2 Pro thermal conductivity meter with a KS-1 sensor (Decagon Devices), a single needle probe 1.2 mm wide and 6 cm long. This commercial stainless-steel needle probe used the short-time solution. A thermistor in the center of the needle samples the temperature every 1 s during a heating cycle and a cooling cycle, each 30 s long. The thermal conductivity is obtained by fitting the time–temperature data to the temperature response equations for heating (Equation (1)) and cooling (Equation (2)) (Carslaw and Jaeger, 1959):

$$\Delta T = -\frac{q}{4\pi k} \text{Ei}\left(\frac{-r^2}{4Dt}\right), 0 < t < t_1, \quad (1)$$

$$\Delta T = -\frac{q}{4\pi k}\left[-\text{Ei}\left(\frac{-r^2}{4Dt}\right) + \text{Ei}\left(\frac{-r^2}{4Dt - t_1}\right)\right], t > t_1, \quad (2)$$

where ΔT (K) is a temperature increase or decrease at distance r (m) from the source, q (W m^{-1}) is the heat rate, t_1 (s) is the heating or cooling time, t (s) is time, k (W m^{-1} K^{-1}) is thermal conductivity, D (m^2 s^{-1}) is thermal diffusivity and $\text{Ei}(x)$ is the exponential integral.

Glycerin (CAS 56-81-5) was used to calibrate the probe. The reference thermal conductivity measurement is $0.282 + 5\%$ W m^{-1} K^{-1} at $22.63°C$ (Decagon Devices). It has a thermal conductivity in a range typical of snow. The

Table 2. Material properties used for the numerical simulations

	Needle (steel)	Air	Glycerin
Density (kg m^{-3})	8000	1.293	1265
Heat capacity (J kg^{-1} K^{-1})	460	1005	2367
Thermal conductivity (W m^{-1} K^{-1})	160	0.0243	0.28

thermal conductivity of snow samples was also measured using a guarded hot-plate apparatus (Köchle, 2009). The mean sample temperature in the hot-plate apparatus was $-15°C$, the sample size was $0.2 \, m \times 0.2 \, m$, and the sample thickness was $0.04–0.06 \, m$. The applied temperature gradient was $20 \, K \, m^{-1}$. The samples were equilibrated within 24–36 hours.

2.4. 2-D numerical model of the needle probe

An axisymmetric two-dimensional (2-D) numerical model (ANSYS version 11.0, Thermal Analysis Guide) was used to analyze the influence of an air gap surrounding the needle in case of a short heating time. The needle-probe geometry and the surrounding materials were represented by plane elements. The element has four nodes with a single degree of freedom, temperature. The outside boundary is represented as a circle and is quasi-infinite. The complex change in porosity around the needle was simplified and modeled as an air gap. An air gap of varying size was inserted between the needle and the outer medium. The needle, the inside of the needle, and the heating power were also simulated, based on the information received from the manufacturer. The different material properties used for the simulation are given in Table 2. We simulated glycerin to validate the numerical model because there is ideal thermal contact between the fluid and the needle.

For the simulations the initial temperature was kept constant for the entire sample. The interior boundary condition in the needle was set to a heat generation rate of $0.6 \, W \, m^{-1}$ during the heating cycle. The simulated thermal conductivity was calculated from the temperature–time heating and cooling curves using a nonlinear least-squares fit to Equations (1) and (2). The width of the air gap used in the simulations was 0.02, 0.05, 0.1, 0.15 and 0.2 mm, consistent with observations from the μCT tests. Vapor heat flow was not modeled.

3. RESULTS

The results show there was structural damage (air gap) around the needle and that this damage could affect the measured thermal conductivity.

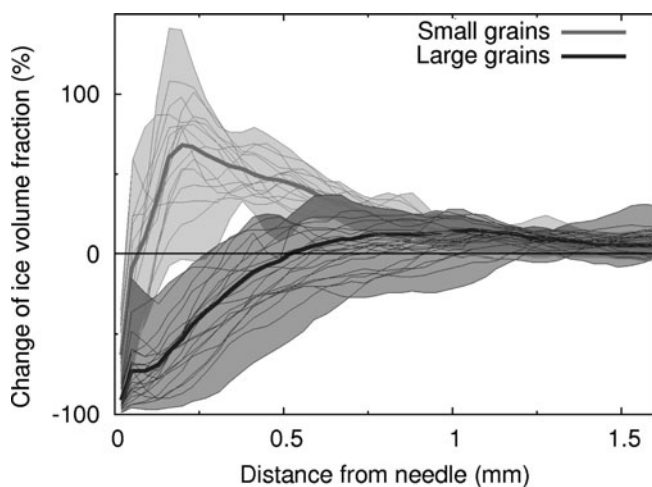## 3.1. Grayscale images and volume fraction evaluation of snow measurements

Figure 2 shows images of two typical experiments with different types of snow. The first image shows small rounded grains (Fig. 2a), and the second large rounded grains (Fig. 2b). The insertion of the needle causes fragmentation of the sintered ice matrix, producing an air gap between the snow and needle. The ice structures fracture at their weakest location and are forced to 'jump' inside the surrounding void space. Because the deformation rate caused by inserting the
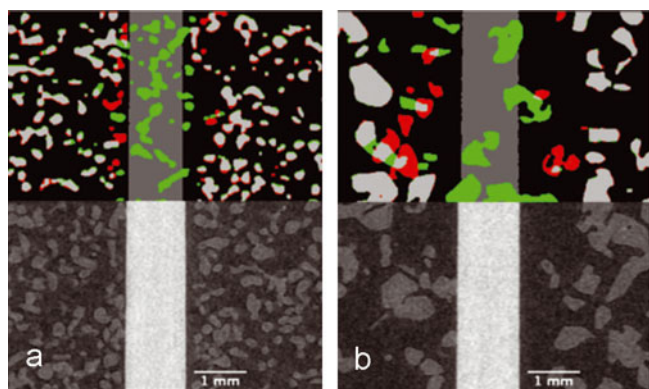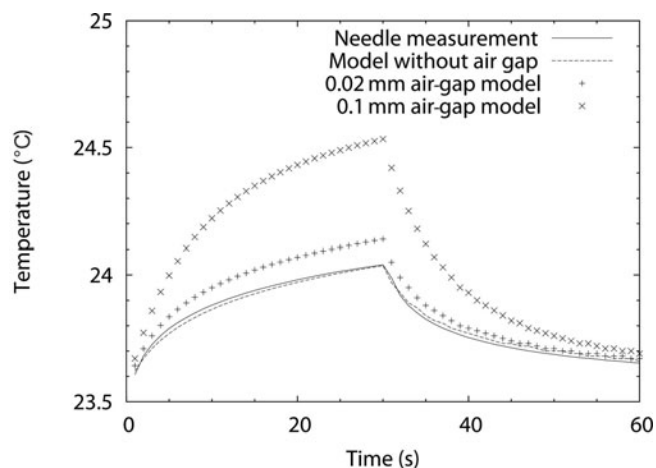
Fig. 2. Change of snow structure due to the needle insertion in (a) small grains (ice fraction 23%, density 213 kg m^{-3}) and (b) large rounded grains (ice fraction 26%, density 239 kg m^{-3}). Upper part of (a) and (b) (difference image between original snow and needle inserted) shows in white: snow not influenced by needle insertion; in green: snow before needle inserted; in red: snow after needle inserted. Lower part of (a) and (b) shows in grayscale the image after needle insertion.
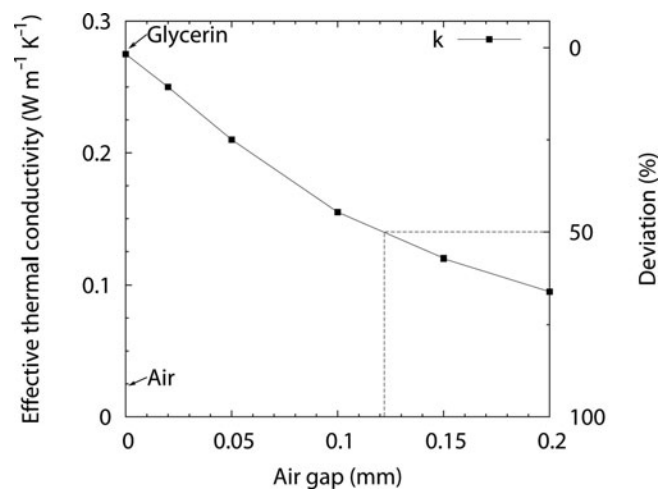

Fig. 4. Measurements and simulation of the thermal conductivity with the needle probe in glycerin. Correspondence of the temperature–time data between the needle-probe device is shown, as well as the effect of air gaps of 0.02 and 0.1 mm around the needle.

needle is high, the ice deforms in an elastic–brittle manner (Johnson and Schneebeli, 1999) and the fracture releases enough elastic energy to cause a particle to travel a considerable distance (~1 mm).

The net result of the radial travel of fractured grains is that the region around the needle has a lower ice fraction than the sample ice fraction (Fig. 3), and a lower ice fraction than before the needle was inserted. Depending mainly on the snow structure, two different types of changes were observed around the needle. Samples with small structures develop a thin air gap with a densified zone up to 0.2 mm surrounding the needle. Samples with larger structures (e.g. depth hoar) show a marked decrease of the volume fraction up to 0.5 mm from the needle, and a much smaller and less distinct densified zone. The disturbance was small beyond 1.2 mm for both types of snow. The same changes were observed after inserting the needle horizontally (data not shown).

3.2. 2-D numerical model of the needle probe with an increasing air gap

For glycerin, the simulations produced results almost identical to those of the measurements made with the KD2 Pro needle probe (Fig. 4). This is the situation where needle and medium are in perfect contact. Thermal conductivities found using the needle-probe measurements, k_n, and the numerical model differed by no more than 5%.

To evaluate the effect of microstructural changes on the measurement of thermal conductivity, we added an air gap to the simulations (Fig. 3). With an air gap present, the temperature of the needle was higher than without an air gap, as expected. The bigger the gap, the higher the temperature. As a result, the air gap altered the simulated temperature–time data (Fig. 4), leading to an apparent decrease in the thermal conductivity. An air gap of 0.02 mm decreased the thermal conductivity by 12.3%, and an air gap of 0.1 mm by 45.6% (Fig. 5).

Fig. 3. Change in the volume fraction of the snow around the needle for the six snow types, measured in two groups. The radius of the cylinder used to measure the change increased by 0.036 mm for each step. 'Large grains' include faceted, large rounded, cup crystals and melt-refrozen grains; 'small grains' include new snow and small rounded grains.

Fig. 5. Simulated absolute and relative effect of an increasing air gap around the needle on effective thermal conductivity, *k*. The material properties of glycerin were used. A 0.1 mm air gap caused a 50% decrease in measured thermal conductivity.

Next, we compared the simulations with the time–temperature curves measured with a needle probe in snow (Fig. 6). The measured temperature–time curve did not correspond to the simulation without an air gap (Fig. 5), using the thermal conductivity calculated from Equations (1) and (2). The main differences between data and simulation occurred during the cooling cycle. The temperature of the simulated needle decreased more slowly than that of the needle probe. This difference in the cooling cycle between measurement and simulation was present for all snow types.

In a final run, we used for the simulation the thermal conductivity of each snow type measured with a guarded plate, k_p. We also added an air gap to the simulation. The thickness of the air gap was adapted to recover the temperature–time curve given by the needle probe. The results (Table 3) are shown for two experiments with small rounded grains (Fig. 6a) and large rounded grains (Fig. 6b).

4. DISCUSSION

The grayscale and binary images (Fig. 2) show that remarkably few direct contacts between the needle and the ice structure exist after inserting the needle. The local ice fraction is much smaller than the initial local ice fraction. This air gap results in simulated thermal conductivities up to 50% lower than they would have been without an air gap.

The formation of this significant air gap is explained by the brittleness of snow structure. The snow structure breaks during the needle insertion and ice particles are forced away from the needle. Because snow is a highly porous material, these particles can be displaced considerably if the material does not have a high density. This is also supported by the structural measurements of ice thickness and pores (Table 2). The mean pore size was at least twice as large as the mean size of ice structures, so the ice could easily move away in the void. During the measurement, the displaced particles will develop only limited bonds (Szabo and Schneebeli, 2007) even in quite warm snow. Our results quantify that the snow structure is disturbed after inserting the needle, increasing the contact resistance.

We observed with our 2-D numerical simulation without an air gap that the behavior of the measured time–temperature curve of the needle probe in the snow does not match the measured values. Using the thermal conductivity measured in a guarded hot-plate apparatus, and adding an air gap in the model, allowed us to recover the temperature–time curve of the measurements. This result is consistent with tomography measurements, and confirms the possibility of an underestimation of the thermal conductivity in porous materials (Abu-Hamdeh, 2001) and the existence of an air gap between the needle and the sample. The air gap of ~0.1 mm cannot be detected by
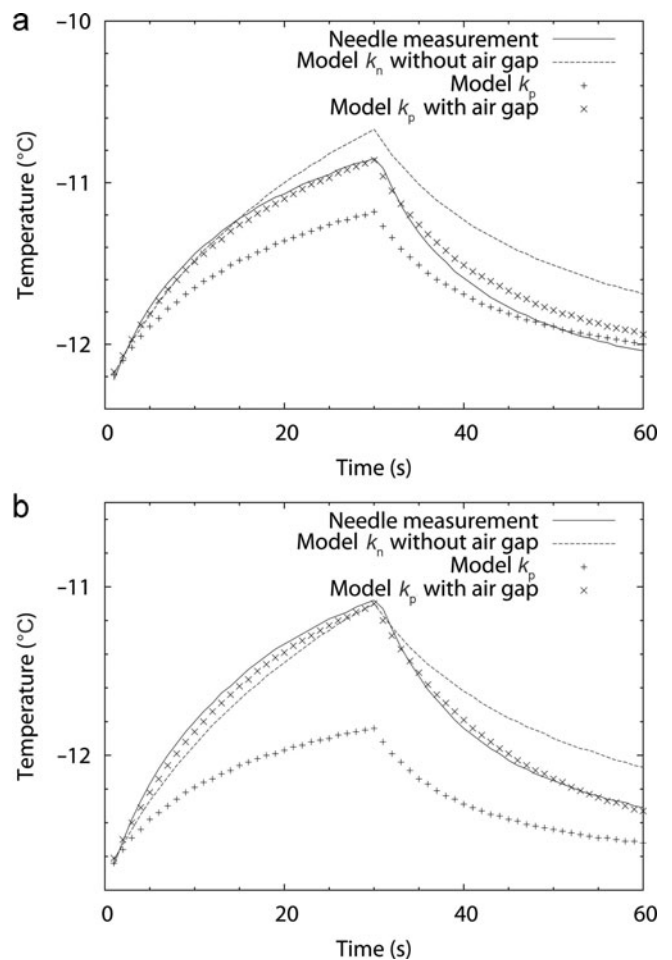
Fig. 6. Evolution of the heating and cooling cycle measured with the needle probe and compared with the numerical model for (a) small rounded grains ($k_n = 0.073 \, \text{W m}^{-1} \text{K}^{-1}$, $k_p = 0.151 \, \text{W m}^{-1} \text{K}^{-1}$) and (b) large rounded grains ($k_n = 0.061 \, \text{W m}^{-1} \text{K}^{-1}$, $k_p = 0.185 \, \text{W m}^{-1} \text{K}^{-1}$). The effective thermal conductivity, k_n, was measured using a needle probe, and k_p using a guarded hot-plate apparatus. The measured time–temperature curve can be recovered by increasing k_n to k_p and adding an air gap.

simple visual observations, because the transparency of ice makes such observations impossible.

The numerical simulation does not help us to find the correct thermal conductivity. However, it allows us to check whether the air gap influences the measurement. The temperature in the cooling cycle recedes faster with an air gap in the simulation than in the measurement. We found no reliable method to determine the air gap for different snow types, so an inverse modeling of the short-term solution is not possible. The formation of an air gap has only a minor effect on the long-term solution.

Table 3. Results for measured thermal conductivities ($\text{W m}^{-1} \text{K}^{-1}$) and values from parameterizations (see also Fig. 5), and the air gap used in the numerical simulation. The columns 'Needle' and 'Plate' are measured. The ISBA (Interactions Soil–Atmosphere–Biosphere) formula is according to Cook and others (2008). The uncertainty of the measured values is around ±10%; no uncertainty is given for ISBA

	Density	Needle	Plate	ISBA	Air gap used in simulation
	kg m^{-3}	W m^{-1} K^{-1}	W m^{-1} K^{-1}	W m^{-1} K^{-1}	mm
Small rounded	213	0.073	0.151	0.159	0.1
Large rounded	239	0.061	0.185	0.190	0.25

It remains an open question whether there are other issues related to using needle probes in porous media. The differences in thermal conductivity of snow used in model parameterizations (e.g. Brun and others, 2008) and the measurements of Sturm and others (1997, 2002) cannot be explained by the formation of an air gap. The reason for the difference remains unresolved for the moment. Possibly, the anisotropic nature of the thermal conductivity in snow (Izumi and Huzioka, 1975) needs to be considered in future experiments. Both solutions, short- and long-term heating, assume that thermal conductivity in the snow is isotropic. If the thermal conductivity is lower horizontally than vertically, the needle probe measures a thermal conductivity value that is too low in the vertical, heat-flow-parallel direction. A needle-probe measurement would then result in a systematically lower value than measured with hot-plate apparatus.

5. CONCLUSION

We show that a needle probe alters the snow microstructure, and, in the case of a short heating time, the resulting thermal conductivity is too low by a factor of 2–3 compared with guarded hot-plate measurements and the parameterization used by snow models. The formation of the air gap around the needle is caused by the very brittle fracture of snow during the rapid insertion of the needle. The existence of such an air gap can be detected in the signature of the measured time–temperature curve and reproduced by numerical simulation. We were not able to propose a method to correct the measured values, because the size of the air gap varies with the microstructure. The results show that contact resistance changes variably in snow, and the thermal conductivities of needle probes with short (30 s) measurement times are biased. This effect can probably also be observed in other brittle and highly porous materials. The needle probe with short heating time cannot be used in snow, and a significantly faster measurement of the thermal conductivity of snow in the field is not possible.

REFERENCES

Abu-Hamdeh, N.H. 2001. Soil and water measurement of the thermal conductivity of sandy loam and clay loam soils using single and dual probes. *J. Agr. Eng. Res.,* **80**(2), 209–216.

Arons, E.M. and S.C. Colbeck. 1995. Geometry of heat and mass transfer in dry snow: a review of theory and experiment. *Rev. Geophys.,* **33**(4), 463–493.

Blackwell, J.H. 1956. The axial-flow error in the thermal-conductivity probe. *Can. J. Phys.,* **34**(4), 412–417.

Brandt, R.E. and S.G. Warren. 1997. Temperature measurements and heat transfer in near-surface snow at the South Pole. *J. Glaciol.,* **43**(144), 339–351.

Bristow, K.L., R.D. White and G.J. Kluitenberg. 1994. Comparison of single and dual probes for measuring soil thermal properties with transient heating. *Austral. J. Soil Res.,* **32**(3), 447–464.

Brun, E., Z.-L. Yang, R. Essery and J. Cohen. 2008. Snow-cover parameterization and modeling. *In* Armstrong, R.L. and E. Brun, *eds. Snow and climate: physical processes, surface energy exchange and modeling.* Cambridge, etc., Cambridge University Press, 125–156.

Carslaw, H.S. and J.C. Jaeger. 1959. *Conduction of heat in solids. Second edition.* Oxford, Clarendon Press.

Cook, B., G. Bonan, S. Levis and H. Epstein. 2008. The thermoinsulation effect of snow cover within a climate model. *Climate Dyn.,* **31**(1), 107–124.

Courville, Z.R., M.R. Albert, M.A. Fahnestock, L.M. Cathles and C.A. Shuman. 2007. Impacts of an accumulation hiatus on the physical properties of firn at a low-accumulation polar site. *J. Geophys. Res.,* **112**(F2), F02030. (10.1029/2005JF000429.)

De Vries, D.A. 1952. A nonstationary method for determining thermal conductivity of soil in situ. *Soil Sci.,* **73**(2), 83–90.

Ewen, J. and H.R. Thomas. 1987. The thermal probe: a new method and its use on an unsaturated sand. *Géotechnique,* **37**(1), 91–105.

Izumi, K. and T. Huzioka. 1975. Studies of metamorphism and thermal conductivity of snow. I. *Low Temp. Sci., Ser. A* 33, 91–102. [In Japanese with English summary.]

Johnson, J.B. and M. Schneebeli. 1999. Characterizing the microstructural and micromechanical properties of snow. *Cold Reg. Sci. Technol.,* **30**(1–3), 91–100.

Kaempfer, T.U. and M. Schneebeli. 2007. Observation of isothermal metamorphism of new snow and interpretation as a sintering process. *J. Geophys. Res.,* **112**(D24), D24101. (10.1029/2007JD009047.)

Kaempfer, T.U., M. Schneebeli and S.A. Sokratov. 2005. A microstructural approach to model heat transfer in snow. *Geophys. Res. Lett.,* **32**(21), L21503. (10.1029/2005GL023873.)

Ketcham, R.A. and W.D. Carlson. 2001. Acquisition, optimization and interpretation of X-ray computed tomographic imagery: applications to the geosciences. *Comput. Geosci.,* **27**(4), 381–400.

Köchle, B. 2009. Thermal conductivity of snow: systematic comparison of measurement methods. (MS thesis, University of Graz.)

Koenig, L.S., E.J. Steig, D.P. Wienbrenner and C.A. Shuman. 2007. A link between microwave extinction length, firn thermal diffusivity, and accumulation rate in West Antarctica. *J. Geophys. Res.,* **112**(F3), F03018. (10.1029/2006JF000716.)

Lange, M.A. 1985. Measurements of thermal parameters in Antarctic snow and firn. *Ann. Glaciol.,* **6**, 100–104.

Nusier, O.K. and N.H. Abu-Hamdeh. 2003. Laboratory techniques to evaluate thermal conductivity for some soils. *Heat Mass Transf.,* **39**(2), 119–123.

Pitman, D. and B. Zuckerman. 1967. Effect of thermal conductivity of snow at –88°, –27° and –5°C. *J. Appl. Phys.,* **38**(6), 2698–2699.

Schneebeli, M. and S.A. Sokratov. 2004. Tomography of temperature gradient metamorphism of snow and associated changes in heat conductivity. *Hydrol. Process.,* **18**(18), 3655–3665.

Sturm, M. and J.B. Johnson. 1991. Natural convection in the subarctic snow cover. *J. Geophys. Res.,* **96**(B7), 11,657–11,671.

Sturm, M., J. Holmgren, M. König and K. Morris. 1997. The thermal conductivity of seasonal snow. *J. Glaciol.,* **43**(143), 26–41.

Sturm, M., D.K. Perovich and J. Holmgren. 2002. Thermal conductivity and heat transfer through the snow on the ice of the Beaufort Sea. *J. Geophys. Res.,* **107**(C10), 8043. (10.1029/2000JC000409.)

Szabo, D. and M. Schneebeli. 2007. Subsecond sintering of ice. *Appl. Phys. Lett.,* **90**(15), 151916. (10.1063/1.2721391.)

Von Herzen, R. and A.E. Maxwell. 1959. The measurement of thermal conductivity of deep-sea sediments by a needle probe method. *J. Geophys. Res.,* **64**(10), 1557–1563.

Zhang, T. 2005. Influence of the seasonal snow cover on the ground thermal regime: an overview. *Rev. Geophys.,* **43**(RG4), RG4002. (10.1029/2004RG000157.)